Finite-Element Modeling of Needle Electrodes in Tissue From the Perspective of Frequent Model Computation

Davorka Šel, Serge Mazeres, Justin Teissie, and Damijan Miklavčič*

Abstract—Information about electric field distribution in tissue is very important for effective electropermeabilization. In heterogeneous tissues with complex geometry, finite-element (FE) models provide one of alternative sources of such information.

In the present study, modeling of needle electrode geometry in the FE model was investigated in order to determine the most appropriate geometry by considering the need for frequent FE model computation present in electroporation models. The 8-faceted needle electrode geometry proposed—determined on a model with a single needle electrode pair by means of criteria function—consisted of the weighted sum of relative difference between measured and computed total current, the relative difference in CPU time spent on solving model, and the relative difference in cross section surface of electrodes. Such electrode geometry was further evaluated on physical models with needle arrays by comparison of computed total current and measured current. The agreement between modeled and measured current was good (within 9% of measurement), except in cases with very thin gel. For voltage above 50 V, a linear relationship between current and voltage was observed in measurements. But at lower voltages, a nonlinear behavior was detected resulting from side (electrochemical) effects at electrode-gel interface. This effect was incorporated in the model by introducing a 50-V shift which reduced the difference between the model and the measurement to less than 3%.

As long as material properties and geometry are well described by FE model, current-based validation can be used for a rough model validation. That is a routine assay compared with imaging of electric field, which is otherwise employed for model validation. Additionally, current estimated by model, can be preset as maximum in electroporator in order to protect tissue against damage.

Index Terms—Finite element modeling, model validation, needle electrodes, tissue permeabilization.

I. INTRODUCTION

ELECTROCHEMOTHERAPY and gene transfer are two promising therapeutic approaches being more and more widely used [1]–[4]. In the case of electrochemotherapy, a cy-

totoxic agent is injected *in vivo* and short high-voltage pulses are applied in order to facilitate transport of cytotoxic drug in tumour cells. This method is already used in clinics [5]–[7]. When gene therapy is concerned, the transfer of DNA material into cells is required. Such a transfer is facilitated by a short high-voltage electric pulse, which permeabilizes cells, followed by a longer low-voltage electrophoretic pulse that does not affect cell permeabilization level but provokes DNA transfer to the cells [8]. The method has been shown to be advantageous compared with viral methods of gene transfection and it has entered preclinical trials [9]. As described, the efficiency of both approaches depends on the same condition: the amount of nonpermeate (cytotoxic drug, DNA, proteins) molecules being transported into cell.

The transfer of nonpermeant molecules or drugs into cell by means of electric field is based on the phenomenon referred to as electropermeabilization or electroporation [10]. Electroporation is an increase in membrane permeability resulting from the application of an external electric field higher than a critical value. This increase in membrane permeability allows molecules and drugs, which cannot cross cell membrane under normal conditions, to enter the cell.

Electropermeabilization depends on membrane properties, cell shape, cell interaction [11], and applied electric pulse properties. A key parameter is the local electric field strength. Since the field results from a voltage applied between the two electrodes, the electrode configuration is clearly controlling the field distribution [12]–[15] and as such the effective uptake. Electrode configurations used for therapeutic purposes are parallel plates, wire and contact plate electrodes, as well as needle electrodes and needle arrays [16]–[18]. Electrode configuration in combination with applied pulses, which are determined by their shape, length, and amplitude [19], results in electric field distribution in tissue. On the other hand, tissue due to its anatomy and its electrical properties [20]–[22] reacts to the applied external electric field. If the applied external electric field is high enough, it results in local permeabilization of the tissue. In [15], it was shown that electric field distribution controls permeabilization. The particular value of the electric field, which is high enough to initialize permeabilization, is called the reversible threshold value [23], [24], due to the fact that after the electric field application the membrane can reseal into its primary state. If the electric field is too high it can cause irreversible change in cell membrane, therefore, such a value is called irreversible threshold value. The importance of adequate

electric field distribution for electroporation was addressed in [14], and [25]–[28].

In clinical applications, it is very important to obtain permeabilized volume, covering whole tissue being subjected to electroporation and at the same time to preserve cells against damage, which could result from too high electric fields. It is, therefore, necessary to choose suitable electrode configuration and pulse parameters for the particular tissue before it is treated. In order to obtain such information, electric field distribution in a tissue must be computed in advance. Such information can be obtained by means of modeling.

Modeling of electric field distribution in tissue is demanding due to heterogeneous tissue properties and usually complex shape. Analytical modeling of such a problem is very difficult if not impossible. Therefore, in most cases numerical modeling techniques are used. Mostly, the finite-element method (FEM) and finite-difference method are applied [28], [29]. Both numerical methods have been successfully used and validated by comparison of computed and measured electric field distribution [15], [23]. FE model validation can be also carried out by comparing total computed current and measured current which is much faster than imaging methods used to validate electric field distribution in tissue. That was demonstrated in [15] where experimental current density obtained by the current density imaging (CDI) method [27] was qualitatively compared with current density obtained by the FE model. The comparison was performed for two different needle electrode sets producing different current densities and electric field distributions. Modeled and measured current densities showed strong correlation for both electrode sets. Also, the total current measured during CDI was very similar to the total current obtained by the FE model for both electrode sets. Therefore, FE model validation with experimental current measurements can be used as a fast method of rough model validation, provided the material properties and geometry are properly described in the model.

On the other hand, it is well known that numerical methods are computationally demanding [30]. Therefore, it is required to search for simplifications in modeling process which can decrease computational efforts and at the same time preserve the accuracy of the result, i.e., electric field distribution. This is of great importance in models of electroporation where frequent computation of electric field is necessary [31]. In this paper, we focus on simplifications, which can be employed to modeling needle electrodes.

Needle electrodes, compared with other electrodes mentioned above, are routinely used in *in vivo* experiments, because a deep penetration of the field is obtained. Needle electrodes are very complex for FE modeling, due to their curved shape and usually large disproportions in terms of size with surrounding tissue. In this study, we have, therefore, investigated how to model needle electrodes in the FE model in order to hasten the solution process. Different needle geometries (4-, 8-, and 12-faceted) were tested on FE model with one pair of needle electrodes. The results were evaluated by comparing computed total current and measured current in tissue phantoms. The proposed needle electrode geometry was then examined in needle arrays with 2–4 pairs of needle electrodes. The results of all examples were val-
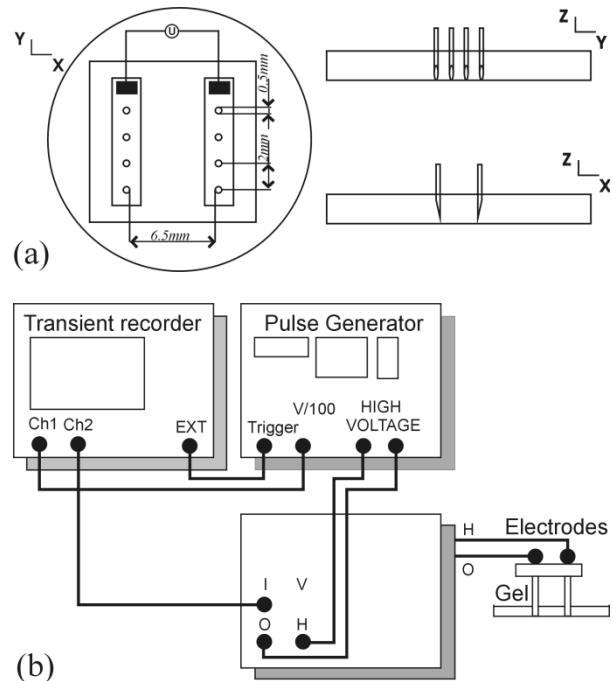
Fig. 1. (a) Position of needle electrodes and holder in Petri dish, view in xy plane (left); yz and zx plane (right). (b) Pulse generator and acquisition unit.

idated by comparison of computed total current and measured current on phantom tissue.

II. MATERIALS AND METHODS

A. Sample

Tissue phantom was used instead of real tissue in all experiments, with electrical parameters and characteristics close to the real tissue. Tissue phantom was made from gelatine (2.4% w/v) in phosphate buffer (concentration: 20 mM; pH= 7.4) and NaCl (concentration: 150 mM). This is actually a gel with some rigidity when cooled. Due to the moisture of the gel, a good electrical contact was obtained with electrodes inserted in the gel. Tissue phantom conductivity was 1.5 S/m. Fresh gel was prepared from a buffer before each experiment and its conductivity was measured.

The phantom tissue was prepared in a Petri dish of 35-mm diameter. The thickness of the gel was either 2, 4, or 6 mm and it was controlled by pouring a given volume of the hot liquid gel in the dish.

B. Electrical Measurements

Needle electrodes were placed in a holder as described in [24] and shown in Fig. 1(a), i.e., nonconductive material with needles in the array placed 2 mm apart. The two arrays were 6.5 mm apart. The arrays had place for up to four needles. Needle diameter was 0.5 mm. The tip of the needle was always in contact with the bottom of the dish. Therefore, the length of the needle in contact with the gel was the same as the thickness of the gel. Needle tips were oriented toward each other as shown in Fig. 3, left.

The voltage pulse was delivered by a high-voltage square wave pulse generator (Jouan PS 10, France). A resistor R (about

1 Ω) was inserted in series with the electrode array to monitor the current. Both, the voltage pulse delivered by the generator and the voltage across the resistor R were digitized (8 bits resolution) and stored on line with a transient recorder (Data Lab DL 905, UK). The stored signals were observed on an oscilloscope and analyzed on a MacIntosh LCIII microcomputer (Apple, USA) by using an ADA4 interface with an Excel subroutine. The system as shown in Fig. 1(b) was calibrated for the current by using an ohmic calibrated high power resistor in place of the needle array. Applied voltage was up to 500 V, in increments of 100 V. The pulse duration was 0.1 ms. By plotting voltage through current (U/I) ratio during the pulse delivery, material conductivity was observed to be constant. Under our experimental condition (sampling rate 1 μs), no delay between voltage and current signals was observed and negligible transient response of current comparing to pulse length was detected, which indicated pure ohmic behavior of the gel. A linear response of the system was observed for increasing values of the applied voltage (up to 1000 V). Lower applied voltages (0–100 V) were studied with increments of 25 V.

C. Experiments

Several experiments with needle electrodes differing in a number of needles, distance between the needles and also gel thickness (2, 4, and 6 mm) were carried out. Each experiment was performed in three replicates, which all together sum up to 50 experiments. Reproducibility of replicate accuracy in each experiment was high, which was the reason to conclude three replicates per experiment were enough.

D. Finite Element Method

A three-dimensional FE model of a gel in Petri dish with inserted needle electrodes was designed using software package Emas produced by ANSOFT Corporation.

The geometry under the study was moderately complex, involving few physical objects (gel and needles) with specific geometrical and material properties. To simplify modeling and solution process, the basis of the FE approach is to divide volume into many FEs, each with much simpler properties. In software package EMAS, when automatic mesh generation is selected, FEs have the shape of tetrahedrons. Material properties within each element are uniform. FEs with additional mid-side node on each element edge are referred to as quadratic elements. The curved element edge option enables mid-side nodes to be placed outside the straight line connecting corner nodes. In this way, the curved element edge can be obtained, which leads in a better representation of curved geometries.

Mesh was denser in regions around electrodes than at the edge of a Petri dish. The reason for such meshing was expected steep change in electric field distribution close to electrodes. Another reason to create denser mesh around electrodes was the dimension of electrodes, which was significantly smaller than dimensions of the surrounding gel.

Our model was described with equations for steady electric current in volume conductor, due to the fact that constant voltage was applied to homogenous and isotropic material with ohmic behavior—gel. Steady electric current in the volume conductor
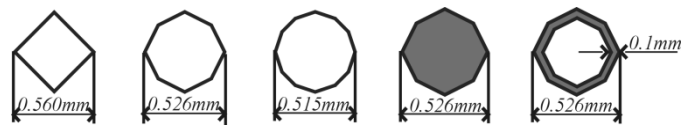
Fig. 2.   Cross section of 4-, 8-, and 12-faceted, solid and tube electrodes.
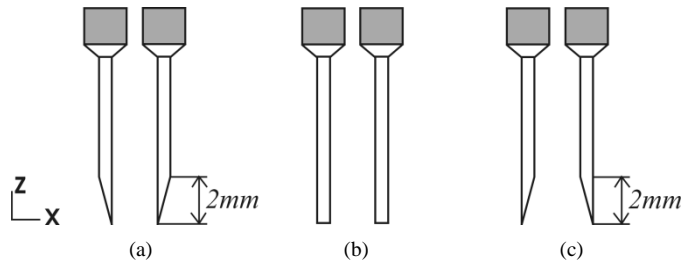
Fig. 3.   Modeling needle electrodes. (a) Tips-in; (b) no tips; and (c) tips-out.

was described by means of Laplace equation. Laplace equation together with two types of boundary conditions, which are Dirichlet boundary condition and Neumann boundary condition, describes electric field inside the volume conductor. The Dirichlet boundary condition, defined as a fixed scalar electric potential (constant voltage), was applied to the surface of the electrodes. Neumann boundary condition, defined as the first derivative of the scalar electric potential in the normal direction to the surface, was automatically set to zero on the outer border of the model.

III. MODELING RESULTS

Modeling of cylindrical shapes with the FEM is a demanding task. Namely, such a shape has to be approximated with a huge number of basic elements such as bricks or tetrahedrons. This problem is usually solved by allowing certain deviation between geometry edge and FE edge, using elements with curved boundaries and by generating very dense mesh in the curved region (at the edge of the electrodes). However, very dense mesh results in computational complexity of models.

Needle electrodes in our model represented a problem of this type. Due to the fact that their size was 70 times smaller than the size of the surrounding gel, a very dense mesh had to be generated in the region around electrodes. Despite using quadratic tetrahedron elements with curved edges, the modeling of cylindrical electrodes was inadequate. A very dense mesh was required to generate a better solution. Therefore, in order to simplify modeling process, we approximated cylindrical electrodes with 4-, 8-, and 12-faceted shapes. The needle tips of 2-mm length were modeled in all needle approximations. Another point was to investigate whether the electrodes could be modeled as hollow or solid or they had to be approximated as tubes having certain thickness of edge, like the needles used in experiments. Fig. 2 shows the 4-, 8-, and 12-faceted electrodes in plane perpendicular to their length, as well as the solid and tube electrode.

Another issue of interest was to determine if modeling of needle tips can be ignored, as shown in Fig. 3(b), or they have to be modeled in such a way as to correspond to real tips, as shown in Fig. 3(a), and to investigate the influence of the tip orientation as shown in Fig. 3(c).

TABLE I
MEASURED CURRENTS AND TOTAL CURRENTS COMPUTED BY MODELS WITH DIFFERENT NEEDLE GEOMETRIES

Thickness of gel (mm)	Current (A)							
	Measurement	4-facet, tips in	8-facet, tips in	8-facet, tips out	12-facet, tips in	Solid, tips in	Tube, tips in	8-facet, no tips
2	1.00	1.23	1.25	1.25	1.26	1.25	1.26	1.38
4	2.60	2.60	2.64	2.63	2.64	2.63	2.64	2.76
6	4.00	3.98	4.02	4.01	4.02	4.01	4.02	4.13

In order to determine which simplifications can be employed without seriously affecting modeling results, we designed all needle geometries mentioned above, computed total current and compared result with current measurements from the experiments. These comparisons were performed on the experiment with a single-needle pair. Based on validation of the results on a single-needle pair, the most adequate needle geometry was selected and used in models with two- to four-needle pairs. In all models, electric field amplitude was observed in two planes, i.e., xy plane, perpendicular to electrodes, 1 mm below the surface and yz plane crossing in the middle between the electrodes.

A. Single Pair of Needle Electrodes

Needle electrode geometries used for simplified representation of cylindrical electrodes were hollow 4-, 8-, and 12-faceted, solid (stainless-steel) and tube electrodes with modeled tips and 8-faceted needles without modeled tips. Due to the fact that in FE model constant voltage was applied to the surface of the electrodes (Dirichlet boundary condition), we preserved the same electrode surface in cases of 4-, 8-, and 12-faceted electrodes, as of cylindrical electrodes ($o = 2\pi r = 1.57$ mm). The inner distance between electrodes was kept constant at 6.5 mm for all electrode geometries. Total currents computed for all types of electrodes and different gel thicknesses are summarized in Table I. The relative difference between measured (y_o) and modeled (y_m) current was expressed as

$$e = \frac{y_o - y_m}{y_o} 100\%. \qquad (1)$$

The relative difference computed by considering currents from Table I showed that different electrode geometries used in FE models did not differ significantly among each other. The maximal difference in relative error amongst models was 3%, except for needles without modeled tips where it was 15%. However, we observed that computed total current significantly differed from the measurement for all experiments with thickness of gel equal to 2 mm. In experiments with thickness of gel equal to 4 and 6 mm, the computed total current with the FE model did not differ from the measured one for more than 2%, except for needles without modeled tips, where it was 6%.

In FE models, the number of FEs or nodes in the model affects the time spent on solving the model [32], because the differential equation is discretized into a series of FE equations, which form a system of linear equations to be solved. Models with needle electrode geometries examined in our study differed also in a number of FEs. The default FE size, which had to be determined according to software package EMAS at the beginning of automatic mesh generation, was the same in all cases. The program itself then generated denser mesh in critical re-

gions, i.e., around curved or smaller objects. The difference in CPU time spent on solving the model with the smallest mesh (CPUtime$_4$)—according to the number of elements that was the mesh in the model with 4-faceted needle electrodes—and CPU time spent for solving other models (CPUtime$_m$) was expressed in relative terms as

$$R_t = \frac{\text{CPUtime}_m - \text{CPUtime}_4}{\text{CPUtime}_4} 100\%. \qquad (2)$$

The largest relative difference was obtained in the model with solid needle electrodes (57%) and the smallest in the model with hollow 8-faceted electrodes (7%), while models with 12-faceted and tube electrodes differed for about 15% and the model with no-tips electrodes for 20%, from the model with 4-faceted needle electrodes. CPU time was measured on the same computer with the same applications running at the time of the FE model computations.

Due to the fact that the distance between inner edges of electrodes was kept constant in all models no matter if they were 4-, 8-, and 12-faceted, the volume of the gel between them was not the same, because needle electrodes differed in cross section surface. The relative difference between the cross section surface of cylindrical electrode and faceted electrodes was expressed as

$$R_S = \frac{S_o - S_m}{S_o} 100\% \qquad (3)$$

where S_o denotes the cross section surface of the cylindrical electrode and S_m denotes the cross section surface of either 4-, 8-, or 12-faceted electrodes. The relative difference R_S was highest in the case of 4-faceted electrodes (22%) and smallest with 12-faceted electrodes (2%), while with 8-faceted electrodes it was 5%.

Based on information gathered on all needle electrode models and the validation of corresponding models with current measurements, we defined the criteria function in order to determine which electrodes were most suitable for implementation in further models. The criteria function was expressed as the weighted sum of absolute values of relative difference between model and measurement e, relative difference in CPU time spent on solving the model R_t, and relative difference in the cross section surface R_S

$$J = w_1|e| + w_2|R_t| + w_3|R_S|. \qquad (4)$$

Table II shows the value of the criteria function for all needle electrode geometries used in models. The smaller the value of criteria function, the better the electrode geometry used. All weights used in criteria function represented in Table II were equal to one. However, if a certain factor in the criteria function

TABLE II
VALUE OF CRITERIA FUNCTION J FOR ALL NEEDLE ELECTRODE GEOMETRIES USED

Thickness of gel (mm)	Criteria function J						
	4-facet, tips in	8-facet, tips in	8-facet, tips out	12-facet, tips in	Solid, tips in	Tube, tips in	8-facet, no tips
2	45	36	34	42	63	42	53
4	22	9	9	5	58	20	22
6	22	12	21	18	62	22	29
Σ	90	57	64	65	183	84	104
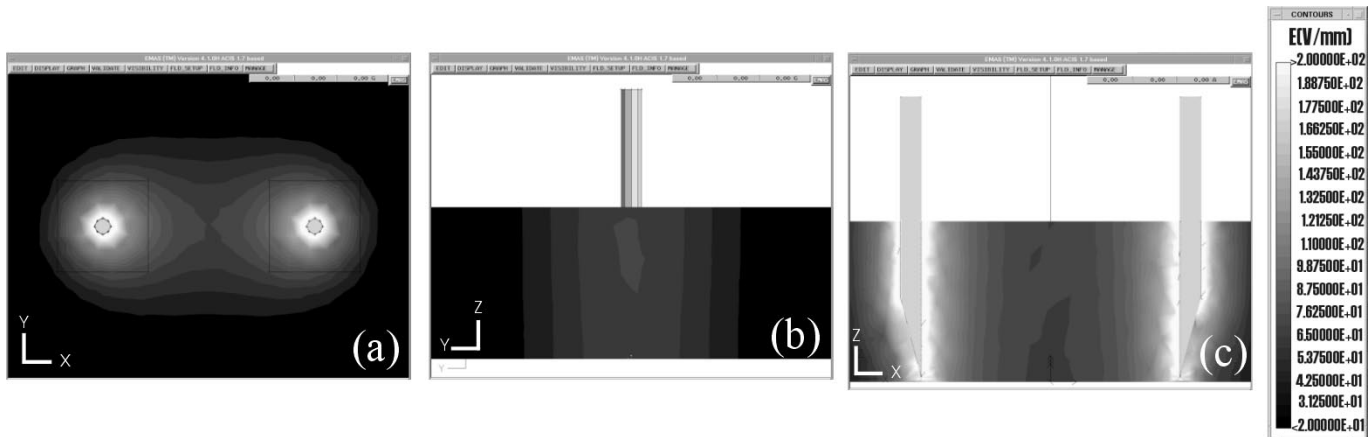
Fig. 4.   Amplitude of electric field computed by model with 8-faceted needle electrodes. Thickness of gel was 4 mm. Voltage applied was 500 V. (a) The xy plane, depth 1 mm below surface; (b) yz plane crossing in the middle between the electrodes; and (c) xz plane.

needs to be exposed, the corresponding weight in criteria function can be changed.

According to the results of criteria function in Table II, the best supplement for cylindrical needle electrodes in FE model were 8-faceted needle electrodes with modeled tips. Furthermore, we observed that tip modeling played a very important role, especially in models with thin gel, where the length of needle tip was equal to the gel thickness, which was the case with 2-mm gel. No significant difference in current was observed between the tip-out and tip-in configurations presented in Fig. 3(a) and (c).

IV. CURRENT-BASED MODEL VALIDATION

Fig. 4 shows electric field distribution computed by a model with 8-faceted needle electrodes in the xy, yz, and xz planes, respectively. Due to the lack of measured electric field distribution, we cannot evaluate the electric field distribution obtained by models in detail. However, in our previous work [15], [23] it was shown that FE models can be efficiently used for computing electric field distribution in tissue around needle electrodes.

Current-based model validation was performed on models with 8-faceted needle electrodes. The first group of measurements used for model validation consisted of needle arrays with 2–4 needle pairs. The two arrays were 6.5 mm apart and the distance between needles in array was always 2 mm. In the second group of measurements—used for model validation only—two-needle pairs were used. The two arrays were again separated by 6.5 mm, however, the distance between neighboring needles in the array was either 2, 4, or 6 mm.

TABLE III
MEASURED AND MODELED CURRENT AND RELATIVE DIFFERENCE BETWEEN THEM FOR NEEDLE ARRAYS. VOLTAGE APPLIED WAS 500 V

Number of electrode pairs	Thickness of gel (mm)	Measurement, Current (A)	Model, Current (A)	Relative error (%)
2	2	1.33	1.86	-40
	4	3.56	3.88	-9
3	2	1.78	2.36	-33
	4	4.45	4.90	-10
4	2	2.44	2.83	-16
	4	5.33	5.78	-8

A.   Needle Arrays With Two, Three, or Four Needles in Array

The results obtained by FE model for the first group of measurements are shown in Table III. Fig. 5 gives the electric field distribution obtained by FE model with 8-faceted needle electrodes for the arrays with 2–4 needle electrode pairs, respectively (in all cases the thickness of gel was 4 mm and voltage applied was 500 V).

Based on the results in Table III, the problem with the discrepancy between the model and measurement persisted in cases with two-and three-needle pairs for the thickness of gel equal 2 mm. However, in the case with four needle electrode pairs and thickness of gel 2 mm the discrepancy between the model and the measurement decreased. Furthermore, the relative difference between the model and the measurement increased to 9% ±1% for all experiments with the thickness of gel equal 4 mm, which was about 7% more than in the model with a single-needle pair used to determine needle geometry for FE modeling. Measurements with 6-mm thickness of gel were not performed, due to safety limitations of the generator.
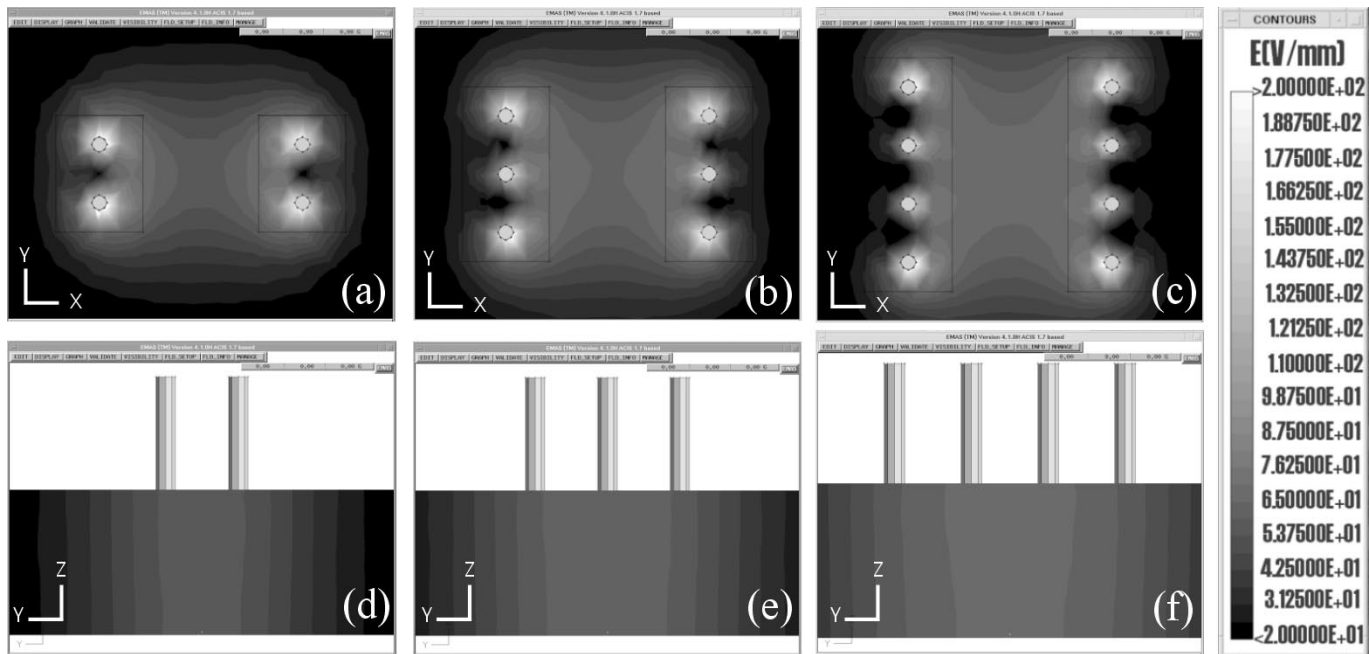
Fig. 5. Amplitude of electric field around two, three, and four-needle pairs approximated by 8-faceted needle electrodes in the FE model in xy plane, i.e., plane perpendicular to the electrodes, depth 1 mm below surface: (a) two-needle pairs; (b) three-needle pairs; and (c) four-needle pairs and in yz plane, crossing in the middle between arrays: (d) two-needle pairs; (e) three-needle pairs; and (f) four-needle pairs. Voltage applied was 500 V.

The degree of electroporation and electric field distribution using needle arrays with four-needle pairs were investigated in [24]. Electric field distribution shown in Fig. 5(c) is comparable with their results.

In Fig. 5, the change in electric field distribution around the electrodes can be observed when additional needle pairs were added. This information is of great importance in cases of electrochemotherapy or gene transfer when predefined volume of tissue needs to be exposed to the electric field greater than the threshold value. As seen in Fig. 5, as the number of needles in the array increases, the electric field between electrodes turns to be more homogenous and higher value of electric field can be obtained between the electrodes. More homogenous electric field distribution with three electrode pairs can also be seen in Fig. 6(a), where comparison of the electric field along the x and along the y axis in the region between the electrodes is shown for one-electrode pair and three-electrode pairs. In Fig. 6(b), the comparison of electric field distribution between one- and four -electrode pairs is shown along y axis.

B. Distance Between Needles in Arrays

Modeling results, i.e., the total current and the relative difference between the model and the measurement for the second group of measurements used for model validation are shown in Table IV. All measurements from second group were performed only with gel of 4-mm thickness. Fig. 7 presents electric field distribution for the cases where two electrode pairs were placed at distances 2, 4, and 6 mm.

Results in Table IV show that the current computed by the model fits the measurement very well. Fig. 7 displays the change in electric field distribution as a result of increment in distance

between the two neighboring needle pairs. By increasing the distance between the needle pairs, the electric field in the middle of the arrays decreases. This result is also observed in Fig. 8 where electric field distribution along x and y axis is shown, in the area between electrodes (distance 0 denotes center between electrodes). If the two needle pairs were placed far apart, interaction between both pairs decreased and finally the two pairs behaved as two independent pairs. This is also shown in Fig. 8(b), where the curve representing $E(y)$ for two-electrode pairs at distance 6 mm already has bimodal distribution. Fig. 9 shows the volume of gel exposed to electric field above the value indicated on x axis. Information in Fig. 7–9 can be used to determine the optimal distance between electrodes to achieve the objective of electropermeabilization (required permeabilized volume of tissue, i.e., the volume exposed to the E above the reversible threshold value).

V. DISCUSSION

As found during the model validation phase, measured current and computed current by FE model differed in cases with gel thickness 2 mm.

In order to obtain deeper insight into reasons for such deviations, we plotted graphs with all current measurements (for all voltages and each gel thickness), along with currents computed by FE model. Due to linear character of the model, results for other voltages than ones presented in Table I, Table III and Table IV were obtained by scaling.

Fig. 10 shows approximation of measured and modeled current with the first-order polynomial (line for the experiments with one-, two-, three-, and four-needle electrode pairs). In the legend, corresponding polynomial coefficients are displayed.
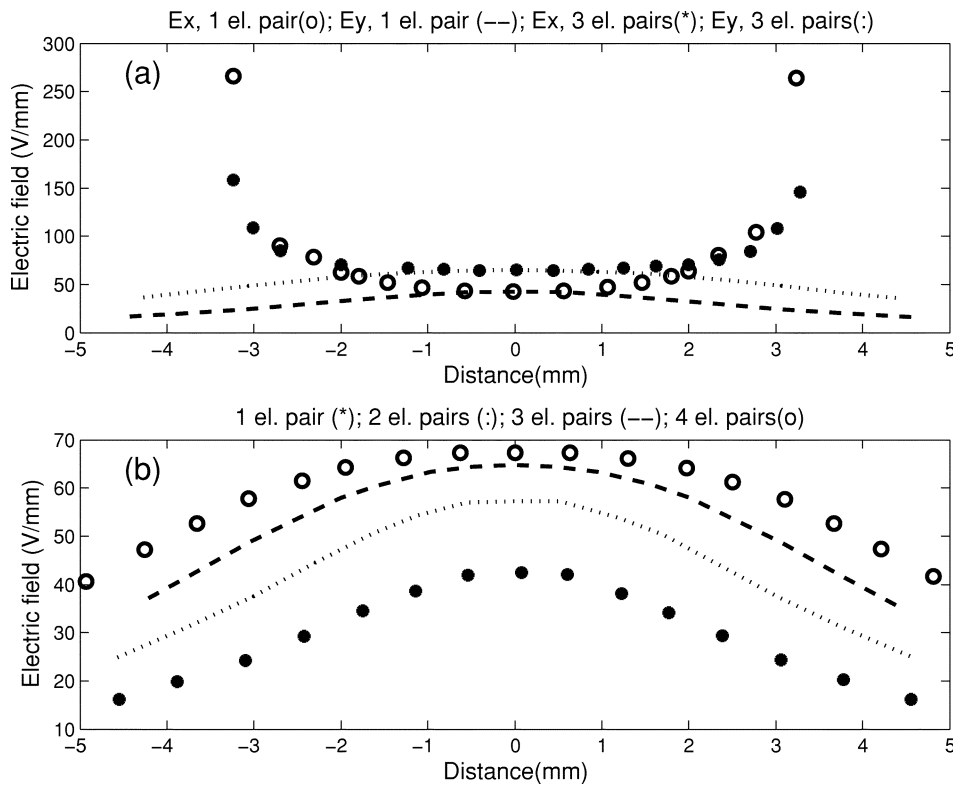
Fig. 6. (a) Comparison $E(x)$ at $y = 0$ and $E(y)$ at $x = 0$ for one-electrode pair and three-electrode pairs. (b) Comparison $E(y)$ for one- to four-electrode pairs. X axis represents distance from the center between electrodes, i.e., at $x = 0$ when $E(y)$ is shown and at $y = 0$ when $E(x)$ is shown. Electrodes placed at $x = -3.5$ and $x = 3.5$ have different polarities.

TABLE IV
MEASURED AND MODELED CURRENT AND RELATIVE DIFFERENCE BETWEEN THEM FOR NEEDLE ARRAYS WITH TWO-NEEDLE PAIRS AND THICKNESS OF GEL 4 MM. VOLTAGE APPLIED WAS 300 V

Distance between needle pairs (mm)	Measurement, Current (A)	Model, Current (A)	Relative error (%)
2	2.30	2.33	-1
4	2.70	2.63	3
6	2.70	2.81	-4

Comparison of both polynomials shows that they have similar slope in all cases. That is also confirmed by equations representing the first-order polynomial

$$y = kx + n \tag{5}$$

where k represents the line slope. The polynomial representing the model always intercepted zero crossing, as expected, while the polynomial representing the measurement always had certain bias, which was the same as constant n in corresponding linear equation. Furthermore, we analyzed possible elements that could cause bias such as the influence of change in thickness of gel, deviations in electrode diameter, and effect of change in distance between arrays and change in distance between two electrode pairs due to possible inaccuracies in experimental setup.

A. Analysis of Measurements on Phantoms

When performing measurements, special attention was paid to several factors in order to provide precise current results. Such factors were, for example, the conductance of the gel, thickness of the gel in the Petri dish, angle between needle electrodes and the gel, and local heating close to the electrodes where the current density is high.

The conductance of gel was controlled by conductometer in a vessel where gel was stored. Before each experiment a fresh gel was poured into a Petri dish from the vessel. During the pulse application plotting of U/I ratio was observed in order to find out if conductance changed during the pulse. Temperature in the laboratory where the experiments were performed was kept constant, which could otherwise affect the conductivity of the gel. Another possible source of measurement error would also be the angle between electrodes orientation and the gel. The angle was adjusted mechanically, which was coarse and, therefore, it could happen that the needle position was not precisely perpendicular to the gel in all experiments.

Change in conductance and deviations in angle between electrodes and gel (i.e., the length of the contact between the gel and the electrodes) contributed mostly to random measurement error, which was determined as negligible. In that respect, also the comparison of measurements and model in Fig. 10 showed influence of bias greater than random error. Namely, slopes of measurement and model polynomials being parallel to each other confirmed that the conductivity used in model was close to the one used in experiments. There were also very small deviations around measurement line which, if they existed, could indicate random measurement error. And, finally, based on the fact that replicate results in all experiments were very close to each other we can conclude that the
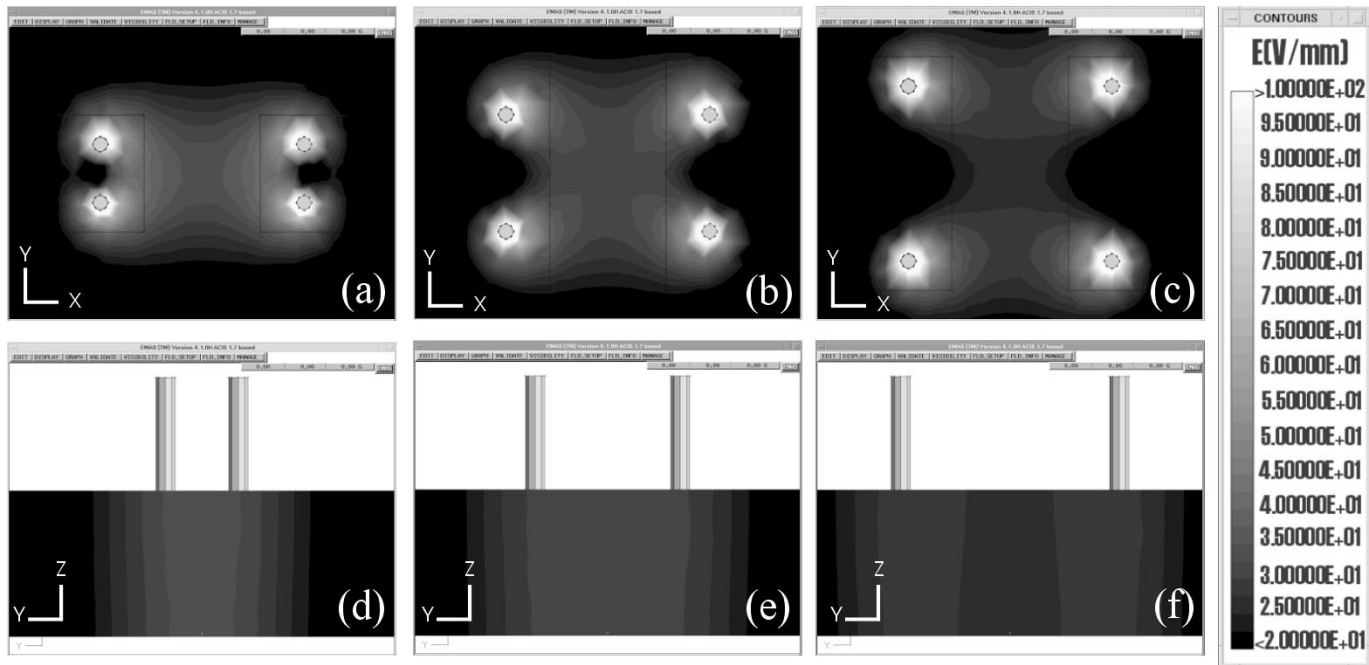
Fig. 7.   Amplitude of electric field around two electrode pairs in xy plane, i.e., perpendicular to the electrodes, depth 1 mm below surface: (a) $d = 2$ mm; (b) $d = 4$ mm; and (c) $d = 6$ mm, and in yz plane, crossing in the middle between arrays: (d) $d = 2$ mm; (e) $d = 4$ mm; and (f) $d = 6$ mm. Voltage applied was 300 V.
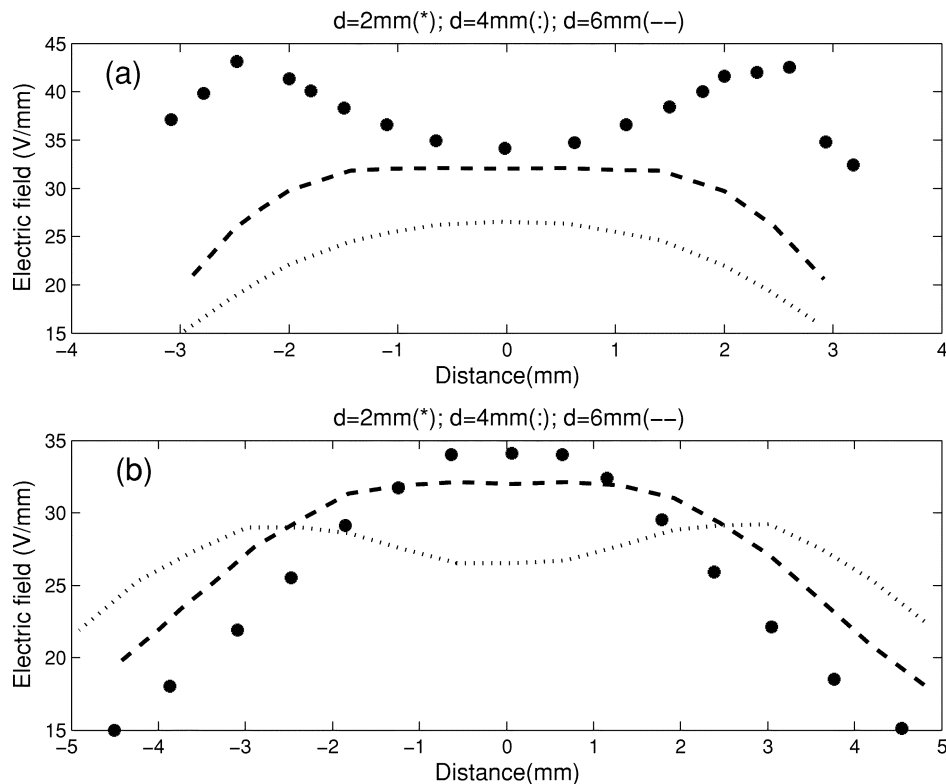
Fig. 8.   (a) $E(x)$ at $y = 0$; and (b) $E(y)$ at $x = 0$ for two-needle pairs, with distance between needles with the same polarity as parameter. X axis represents distance from the center between electrodes, i.e., at $x = 0$ when $E(y)$ is shown and at $y = 0$ when $E(x)$ is shown. Electrodes placed at $x = -3.5$ and $x = 3.5$ have different polarities.

random measurement error was negligible. The total measurement error—which consists of bias and random error—was, therefore, equal to bias error.

Possible source of bias error could be small deviations in thickness of gel, and deviations in distance between electrodes and in distance between arrays which depended on the accuracy of holder dimensions. Another possible source of bias error could be electrode polarization [33], which could have decreased measured current comparing to modeled current. All the potential contributions were checked systematically.
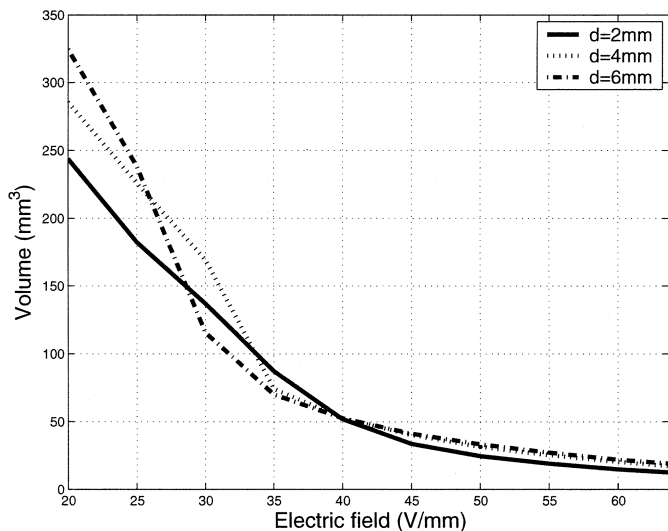
Fig. 9. Volume of gel exposed to electric field above electric field amplitude indicated on x axis. Voltage applied was 300 V. Total volume of gel observed was 2450 mm^3.

1) Thickness of Gel: A critical control was to check the thickness of the phantom. As described in the Materials and Methods part, the thickness of the gel was obtained from the values of the volume of the liquid gel. This was measured at 37 °C. Due to the temperature dilatation coefficient of the gel and of the pipette, some inaccuracies might be present in the effective values of the volume and as such in the thickness after cooling to 20 °C. This was checked by mechanical means with a precision of 0.2 mm. All thicknesses were correct in the central part of the dish within this precision. But due to a meniscus effect, the gel was thicker along the edge of the dish. Therefore, all electrical measurements were run by inserting the electrodes only in the central part of the gel. We checked the effect of small changes of the thickness (± 0.2 mm) on the computed current for a 500-V pulse using the two needle electrode setup. As shown in Table V, a good improvement in the fit between measurements and simulations, provided the thickness decreased was obtained with the thin gel (2 mm), while it increased the difference with thicker gel (4 and 6 mm).

2) Electrode Diameter: Simulations were run under the assumption that the electrode diameter was different than declared. No significant change in the relative difference between experiments and simulation (up to 3%) was obtained for the three different gel thicknesses, provided that relative change in electrode diameter was within $\pm 10\%$.

3) Distance Between Arrays: As the electrode holder was mechanically drilled, some imperfections were present in the distance between the two electrodes. This was introduced in the model but was observed not to improve significantly the relative differences (improvement up to 2%) provided the distance between arrays was changed for $\pm 5\%$.

4) Distance Between Two Electrode Pairs: For the same technical reason, it was checked if the distance between electrodes in an array might alter the simulated current. The distance between two electrode pairs was altered up to $\pm 5\%$. Again no significant improvement in the relative difference was detected (improvement up to 1%).

5) Low-Voltage Results and Voltage Shift: A 0.1-ms pulse with different low voltages was applied to a two-needle electrode setup inserted in a 6-mm gel. As shown in Fig. 11, a nonlinear dependence of the current on the applied voltage, when less than 50 V, was observed. No current flowed between the electrodes when 25 V were applied. A sharp increase was only observed when the voltage was above 50 V. Nonlinear current-voltage dependency indicated the electrode polarization effect. Based on the results at low voltages shown in Fig. 11, a 50-V shift (simulating electrochemical effects at tissue–electrode interface) was added in the model. A significant improvement in fit between the model and the measurement in the current-voltage plot was obtained whatever the electrode array or the gel thickness as shown in Fig. 10. The 50-V shift was introduced in the models only when voltage above nonlinear part of current-voltage dependency was used.

Electrochemical effects at the electrode–tissue interface are in general influenced by electrode chemical nature, sample composition and electrical parameters. In [34], it was shown for aluminum electrodes that calculated electric field (E) using electrode voltages and geometries alone could be significantly higher than the real E present in the tissue. In [35], it was also presented that aluminum electrodes demonstrate higher electrochemical effects than stainless-steel electrodes. Thus, the voltage drop at the electrode-tissue interface needs to be evaluated and correction for electrochemical effects needs to be taken into account in models, which in our model was introduced with 50-V shift.

B. Analysis of Reason of Modeling Error

In our FE models, cylindrical needle electrodes were simplified by 8-faceted electrodes. Our analysis of optimal needle electrode geometry has shown that 12-faceted electrodes, which were closer to cylindrical electrodes, did not perform better than 8-faceted electrodes regarding current relative difference. Therefore, we assumed that this approximation did not bring significant part in modeling error.

On the other hand, comparison of 8-faceted needles with modeled tips and without modeled tips has shown, that tip modeling significantly affected current at 2-mm gel thickness. Tip modeling could be, therefore, one of the reasons for discrepancy in modeled and measured current at 2-mm gel thickness. However, further improvement in tip modeling would not bring additional improvement because tip-in and tip-out orientation did not give significantly different results.

Another source of modeling error could also be the mesh density. Namely scarce mesh could give distorted results. In FE modeling it was, therefore, important to recompute the same model with different mesh densities. Our results with different mesh densities did not differ significantly, so we assumed that mesh densities used were sufficiently high.

VI. CONCLUSION

The method of modeling needle electrodes in FE model, which hastened the solution process was proposed and evaluated by measurements on a phantom tissue. Based on the results of criteria function 8-faceted needle electrodes were
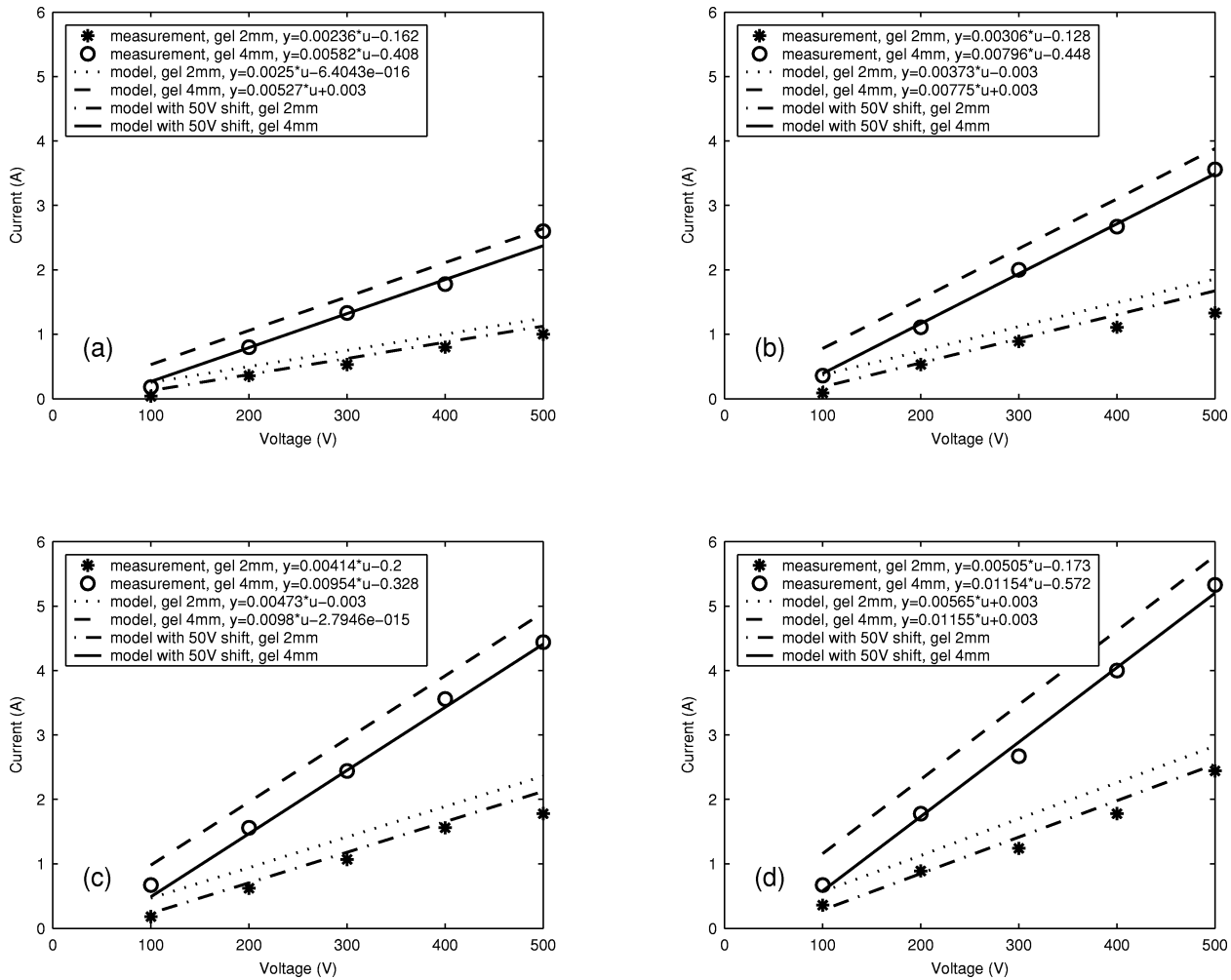
Fig. 10. Measured, computed current and computed current with a 50-V shift added to model: (a) one-needle pair; (b) two-needle pairs; (c) three-needle pairs; (d) four-needle pairs. Gel thickness was either 2 or 4 mm. Measurements are fitted with first-order polynomial, whereas modeled currents are computed by scaling modeled current obtained at 500 V.

TABLE V
SIMULATED VARIATIONS IN THICKNESS OF GEL

Thickness of gel (mm)	Current (A)		Thickness of gel (mm)	Current (A)	Thickness of gel (mm)	Current (A)
	Measurement	8-facet		8-facet		8-facet
2	1.00	1.25	1.8	1.13	2.2	1.37
4	2.60	2.64	3.8	2.51	4.2	2.76
6	4.00	4.02	5.8	3.89	6.2	4.14

proposed as a substitute for cylindrical ones. Results showed that such simplification could be used without serious impact on model results.

The model relative difference in total current, which was evaluated during model validation on measurements, was 9% for gel thickness 4 mm. This difference was not due to approximation of needles with faceted shape neither could be explained by geometrical inaccuracies (gel thickness, tip modeling, and inter-electrode distance) between the model and the real system. The bias was due to the low-voltage behavior which was nonohmic. This could not be predicted by the simulation. However, based on low-voltage measurements, a 50-V voltage shift was introduced in the model and bias error was sharply decreased for applied voltage larger than 100 V. The relative difference between

modeled and measured current decreased from 9% to 3% for gel thickness 4 mm.

Current measurement was also examined as means of FE model validation [15]. Provided model geometry and material properties are know and properly modeled, FE model producing current results which correspond to measured results could be used for at least rough estimation of electric field distribution in tissue. This information is of great importance for effective tissue electroporation in electrochemotherapy and *in vivo* tissue gene transfection. Based on known E distribution, also pulse parameters (especially amplitude) and needle electrodes position could be optimized.

Additionally, such FE model could be used for estimation of maximal current, for different needle electrode geometries and
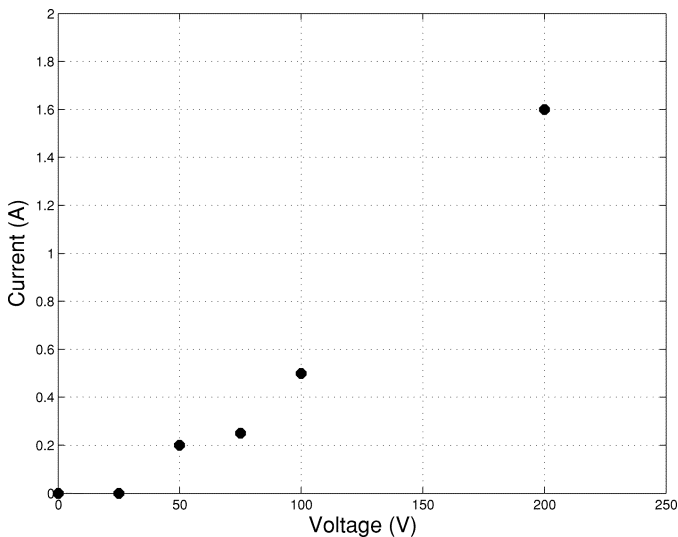
Fig. 11.   Current under low-voltage pulse conditions. Thickness of gel was 6 mm.

given tissue properties (geometry, conductivity). The maximal current could be determined and preset in the electroporator in order to protect the tissue against damage. The maximal current and required voltage for effective tissue electropermeabilization at given electrode geometry are also important in designing electroporators power supply and capacity.

REFERENCES

[1] L. M. Mir, S. Orlowski, J. Belehradek Jr., J. Teissies, M. P. Rols, G. Serša, D. Miklavcic, R. Gilbert, and R. Heller, "Biomedical applications of electric pulses with special emphasis on antitumor electrochemotherapy," *Bioelectrochem. Bioenerg.* , vol. 38, pp. 203–207, 1995.

[2] M. Jaroszeski, R. Gilbert, and R. Heller, "Electrochemotherapy: An emerging drug delivery method for the treatment of cancer," *Adv. Drug Delivery Rev.*, vol. 26, pp. 185–197, 1997.

[3] R. Heller, M. Jaroszeski, J. Leo-Messina, R. Perrot, N. Van Voorhis, D. Reintgen, and R. Gilbert, "Treatment of B16 mouse melanoma with the combination of electropermeabilization and chemotherapy," *Bioelectrochem. Bioenerg.*, vol. 36, pp. 83–87, 1995.

[4] L. M. Mir, "Therapeutic perspectives of in vivo cell electropermebilization," *Bioelechem.*, vol. 53, pp. 1–10, 2000.

[5] G. Serša, B. Štabuc, M. Cemazar, D. Miklavcic, and Z. Rudolf, "Electrochemotherapy with cisplatin: Clinical experience in malignant melanoma patients," *Clin. Cancer Res.*, vol. 6, pp. 863–867, 2000.

[6] G. Serša, B. Štabuc, M. Čemažar, B. Jančar, D. Miklavčič, and Z. Rudolf, "Electrochemotherapy with cisplatin: Potentiation of local cisplatin antitumor effectivness by application of electric pulses in cancer patients," *Eur. J. Cancer*, vol. 34, pp. 1213–1218, 1998.

[7] L. M. Mir, P. Devauchelle, F. Quintin-Colonna, F. Delisle, S. Doliger, D. Fradelizi, J. Belhradek, and S. Orlowski, "First clinical trial of cat soft-tissue sarcomas treatment by electrochemotherapy," *Br. J. Cancer*, 1997.

[8] S. Satkauskas, M. F. Bureau, M. Puc, A. Mahfoudi, D. Scherman, D. Miklavcic, and L. M. Mir, "Mechanisms of in vivo DNA electrotransfer: Respective contributions for cell electropermeabilization and DNA electrophoresis," *Molec. Therapy*, vol. 5, pp. 1–8, 2002.

[9] M. P. Rols, C. Delteil, M. Golzio, P. Dumond, S. Cros, and J. Teissie, "In vivo electrically mediated protein and gene transfer in murine melanoma," *Nat. Biotechnol.*, vol. 16, pp. 168–171, 1998.

[10] J. C. Weaver and Y. A. Chizmadzhev, "Theory of electroporation: A review," *Bioelectrochem. Bioenerg.*, vol. 41, pp. 135–160, 1996.

[11] M. Pavlin, N. Pavšelj, and D. Miklavčič, "Dependence of induced transmembrane potential on cell density, arrangement, and cell position inside a cell system," *IEEE Trans. Biomed. Eng.*, vol. 49, pp. 605–612, June 2002.

[12] J. Gehl and L. L. Mir, "Determination of optimal parameters for in vivo gene transfer by electroporation, using a rapid in vivo test for cell peremabilization," *Biochem. Biophys. Res. Comm.*, vol. 261, pp. 377–380, 1999.

[13] M. R. Prausnitz, C. D. Milano, J. A. Gimm, R. Langer, and J. C. Weaver, "Quantitative study of molecular transport due to electroporation: Uptake of bovine serum albumin by erythrocyte ghosts," *Biophys. J.*, vol. 66, pp. 1522–1530, 1994.

[14] D. Miklavcic, "Electrodes and corresponding electric field distribution for effective in vivo electroporation ," in *Proc. Medicon Conf.*, 2001, pp. 5–9.

[15] D. Miklavčič, K. Beravs, D. Šemrov, M. Čemažar, F. Demšar, and G. Serša, "The importance of electric field distribution for effective in vivo electroporation of tissues ," *Biophys. J.*, vol. 74, pp. 2152–2158, 1998.

[16] M. J. Jaroszeski, R. A. Gilbert, and R. Heller, "In vivo antitumor effects of electrochemotherapy in a hepatoma model," *Biochim. Biophys. Acta*, vol. 1334, pp. 15–18, 1997.

[17] L. H. Ramirez, S. Orlowski, D. An, G. Bindoula, R. Dzodic, P. Ardouin, C. Bognet, J. Belehradek Jr, J. N. Munek, and L. M. Mir, "Electrochemotherapy on liver tumours in rabbits," *Br. J. Cancer*, vol. 77, pp. 2104–2111, 1998.

[18] R. A. Gilbert, M. J. Jaroszeski, and R. Heller, "Novel electrode designs for electrochemotherapy," *Biochim. Biophys. Acta.*, vol. 1334, pp. 9–14, 1997.

[19] J. Teissie and C. Ramos, "Correlation between electric field pulse induced long-lived permeabilization and fusogenicity in cell membranes," *Biophys. J.*, vol. 74, pp. 1889–1898, 1998.

[20] U. Pliquett, E. Gersing, and F. Pliquette, "Evaluation of fast time-domain based impedance measurements on biological tissue," *Biomed. Technik*, vol. 45, pp. 6–13, 2000.

[21] T. J. C. Faes, H. A. van der Meij, J. C. de Munck, and R. M. Heethaar, "The electric resistivity of human tissues (100 Hz–10 MHz) a meta-analysis of review studies," *Physiol. Meas.*, vol. 20, pp. R1–R10, 1999.

[22] V. Raicu, T. Saibara, and A. Irimajiri, "Dielectric properties of rat liver in vivo: A noninvasive approach an open-ended coaxial probe at audio/radio frequencies," *Bioelectrochem. Bioenerg.*, vol. 47, pp. 325–332, 1998.

[23] D. Miklavčič, D. Šemrov, H. Mekid, and L. M. Mir, "A validated model of in vivo electric field distribution in tissue for electrochemotherapy and for DNA electrotransfer for gene therapy," *Biochim. Biophys. Acta*, vol. 1523, pp. 73–83, 2000.

[24] J. Gehl, T. H. Sorensen, K. Nielsen, P. Raskmark, S. L. Nielsen, T. Skorvsgaard, and L. M. Mir, "In vivo electroporation of skeletal muscle: Threshold, efficacy and relation to electric field distribution," *Biochim. Biophys. Acta*, vol. 1428, pp. 233–240, 1999.

[25] G. A. Hofmann, S. B. Dev, and G. S. Nanda, "Electrochemotherapy: Transition from laboratory to the clinics," *IEEE Eng. Med. Biol. Mag.*, vol. 15, pp. 124–132, 1996.

[26] G. A. Hofmann, S. B. Dev, S. Dimmer, and G. S. Nanda, "Electroporation therapy: A new approach for the treatment of head and neck cancer," *IEEE Trans. Biomed. Eng.*, vol. 46, pp. 752–759, June 1999.

[27] I. Serša, K. Beravs, N. J. F. Dodd, D. Miklavcic, and F. Demsar, "Electric current density imaging of mice tumors," *Magn. Res. Med.*, vol. 37, pp. 1–7, 1997.

[28] K. Brandinsky and I. Daskalov, "Electrical field and current distributions in electrochemotherapy," *Bioelectrochem. Bioenerg.*, vol. 48, pp. 201–208, 1999.

[29] D. Šemrov and D. Miklavčič, "Calculation of the electrical parameters in electrochemotherapy of solid tumors in mice," *Computers in Biology and Medicine*, vol. 28, pp. 439–448, 1998.

[30] *EMAS Version 4 User's Manual*, J. R. Brauer and B. S. Brown, Eds., 1997.

[31] R. V. Davalos, B. Rubinsky, and D. M. Otten, "A feasibility study for electrical impedance tomography as a means to monitor tissue electroporation for molecular medicine," *IEEE Trans. Biomed. Eng.*, vol. 49, pp. 400–403, Apr. 2002.

[32] S. Polstyanko and J.-F. Lee, "Fast Schwartz-type finite element electrostatic solver," *IEEE Trans. Magn.*, vol. 37, pp. 3469–3473, Sept. 2001.

[33] R. Plonsey, *Bioelectric Phenomena*.   New York: Mcgraw Hill, 1969, pp. 23–77.

[34] U. Pliquett, E. A. Gift, and J. C. Weaver, "Determination of the electric field and anomalous heating caused by exponential pulses with aluminum electrodes in electroporation experiments," *Bioelectrochem. Bioenerg.*, vol. 39, pp. 39–53, 1996.

[35] F. Loste, N. Eynard, and J. Teissie, "Direct monitoring of the field strength during electropulsation," *Bioelectrochem. Bioenerg.*, vol. 47, pp. 119–127, 1998.

Davorka Šel was born in 1970. She received the B.Sc. and the M.Sc. degrees in electrical engineering from the University of Ljubljana, Ljubljana, Slovenia. Currently, she is working towards the Ph.D. degree in electrical engineering at the University of Ljubljana.

Her main research interest is in the field of electroporation, numerical modeling of electric field distribution in tissue during electroporation, and optimization of electroporation parameters.

Justin Teissie was born in 1947. He received the Ph.D. degree in macromolecular chemistry from the University of Paris, Paris, France, in 1973 and the Ph.D. degree in biophysics from the University of Toulouse, Toulouse, France, in 1979.

Since 1991, he is Director of Research with the CNRS Institute of Pharmacology and Structural Biology, Toulouse. He is the author of more than 200 papers. His main research interests are in the fields of biophysics of biological membranes, fluorescence spectroscopy and video imaging of membranes, and electropulsation of cells and tissues with biomedical and biotechnical applications.

Serge Mazeres received the Ph.D. degree in biophysics from the Paul Sabatier University, Toulouse, France, in 1997.

He worked as a Post-doc at the University of Groningen, Groningen, the Netherlands, in the field of crystal growth followed by atomic force microscopy in the physiological environment. Currently, he is a Research Engineer with the Institute of Pharmacology and Structural Biology, Toulouse, France. He works in the biophysics field maintaining and developing setups on a spectroscopy platform.

Damijan Miklavčič was born in 1963 in Ljubljana, Slovenia. He received the M.Sc. and Ph.D. degrees in electrical engineering from the University of Ljubljana.

Since 2002, he is a Professor with the Faculty of Electrical Engineering, University of Ljubljana, and the Head of Laboratory of Biocybernetics since 1997. He works in the field of biomedical engineering. His interest in the last years focuses on electroporation assisted drug and gene delivery, including cancer treatment by means of electrochemotherapy, tissue oxygenation, and modeling.